Extraction of Fringing-Effect Power Loss from Total Dissipation in Magnetic Component

Rafał Kasikowski
Lodz University of Technology, Faculty of Electrical, Electronic, Computer and Control Engineering, Institute of Electronics, al. Politechniki 10, 93-590 Łódź

Abstract: Power magnetics in the energy storage configuration are not able to handle a significant amount of power without the introduction of a physical discontinuity in their magnetic path. This frequently takes the form of a discrete air gap giving rise to certain consequences such as extra power dissipation in the coils mounted on gapped cores. The ascertainment of the impact of the fringing magnetic field at the air gap on the efficiency of power conversion is highly problematic due to the complex nature of the phenomenon. The fringing-effect power loss typically coexists and is combined with all the other power-dissipation mechanisms, which greatly complicates the extraction of losses brought about solely by the fringing flux at the air gap from the total amount of dissipation in a given magnetic component. Magnetic cores of composite materials do not require a discrete air gap, as the air gap in them is distributed throughout the entire material, thus preventing the fringing magnetic flux from forming. However, there is a downside to this approach, as power loss in the material is comparably greater and so are the manufacturing costs. As shown here, distributed-gap-type core materials, due to the absence of physical discontinuity, and hence the lack of registerable fringing-effect power loss, can be utilized to comparatively ascertain and extract the extra power dissipation due to the fringing effect phenomenon in gapped magnetic components.

Keywords: inductors, transformers, thermography, power losses

1. Introduction

Fringing-effect power loss originates from the magnetic field lines at the air gap looping outside the intended magnetic circuit and crossing adjacent conductors (Fig. 1). This coupling induces undesirable eddy currents that counteract the useful current, hence reducing the effective area of the conductor and increasing the power loss [1, 2]. The described phenomenon is one of three distinct mechanisms behind the induction of eddy currents in conducting materials. At low frequency, current is distributed homogenously throughout the conductor, and power is dissipated in the form of heat due to the so-called DC resistance of the path opposing the current flow. At high frequency, magnetic field lines originating from the current flowing through a conductor cross the conductor and cause eddy currents to occur within it. These currents tend to reduce the net current density in the centre of the conductor but reinforce the current flowing at the surface. This specific eddy-current mechanism is known as the skin effect. The current distribution within the conductor can be obtained by utilization of Maxwell's equations [3]. The obtained results show that the current decays exponentially if progressing downwards from the surface toward the centre. This heterogenous distribution of the current throughout the conductor decreases the effective cross-sectional area of the conductor, hence the increased power loss at high frequency.

Another high-frequency eddy-current mechanism is referred to as the proximity effect, and is particularly evident in conductors that are brought into the immediate vicinity of one another. As in the case of the fringing and the skin effect, the magnetic field lines looping out of the conductors induce eddy currents in the neighbouring conductors and, as a result, the distribution of current density within each of the conductors is altered [4]. Consequently, the proximity effect decreases the available cross-sectional area by concentrating the current in smaller sections of the conductors which in turn causes excess power loss.

The described power-loss mechanisms usually coexist and are combined with each other in every magnetic component with a discrete air gap. The fringing-flux-driven eddy currents are concurrent with the eddy currents brought about by the skin and the proximity effect. As a result, the total power dissipated in the windings is a derivative of all the eddy-current mechanisms, and hence the extraction of losses due to the fringing-effect phenomenon is highly complex. Examining the magnetic field

Autor korespondujący:
Rafał Kasikowski, rafal.kasikowski@p.lodz.pl

Artykuł recenzowany
nadesłany 06.07.2023 r., przyjęty do druku 23.10.2023 r.

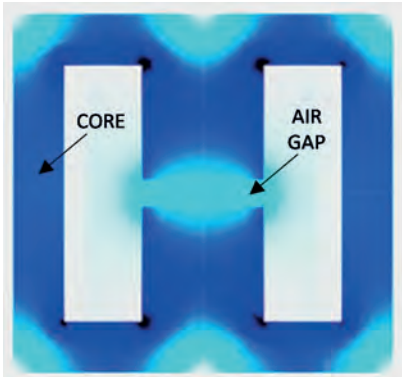

Fig. 1. Visualization of magnetic field density distribution in gapped magnetic component
Rys. 1. Wizualizacja rozkładu pola magnetycznego w elemencie indukcyjnym ze szczeliną powietrzną

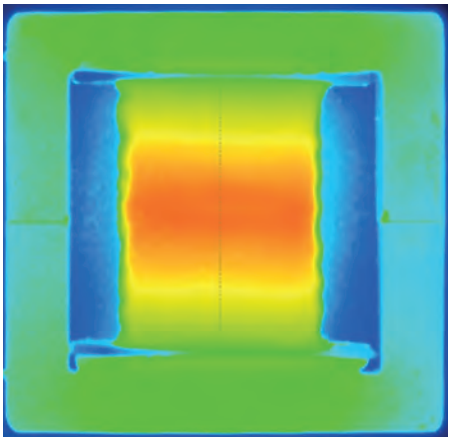

Fig. 2. Thermal image of inductor with air gap
Rys. 2. Obraz termowizyjny elementu indukcyjnego ze szczeliną powietrzną

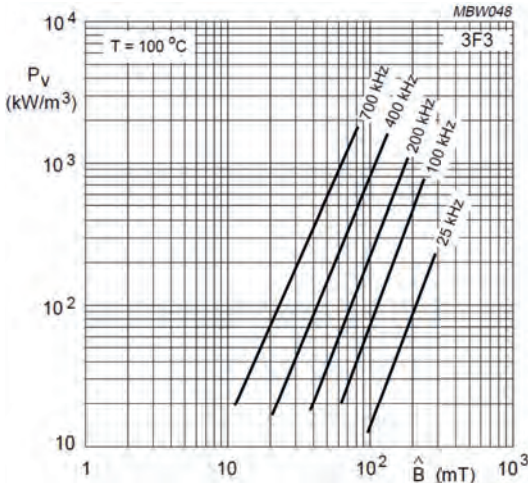

Fig. 3. Total core loss per unit volume as function of frequency and peak magnetic flux density for 3F3 ferrite material [5]
Rys. 3. Całkowite straty mocy w rdzeniu na jednostkę objętości w funkcji częstotliwości i maksymalnej indukcji magnetycznej dla materiału ferrytowego typu 3F3

distribution around the air gap in Fig. 1 one can infer that the fringing-effect loss ought to be localized and largely restricted to the immediate vicinity of the air gap. This conclusion is indeed correct, as illustrated by the thermal image of an inductor with an air gap in Fig. 2. Since power is dissipated as heat, thermographic imaging provides a perfect visualization of losses in the windings of magnetic components.

Power loss is not restricted to the windings and a significant portion of the total loss can be attributed to power-dissipation mechanisms in magnetic cores. The manufacturers of magnetic materials frequently represent the core loss density in the form of figures containing total core loss data as a function of sinusoidal excitation frequency f and magnetic flux density ΔB (Fig. 3).

The graphs can be approximated by the Steinmetz empirical formula Eq. 1 [6].

$$P_V = k_f \cdot f^x \cdot \Delta B^y \tag{1}$$

where k_f, x, y are the ferrite material's coefficients; f is the operating frequency of a given magnetic component; ΔB is the peak AC magnetic flux density

One can note that the core loss density graphs in Fig. 3 are drawn for temperature $T = 100\,°\text{C}$. The extended version of the Steinmetz formula is applicable to a wider range of operating temperatures, Eq. 2.

$$P_V = k_f \cdot f^x \cdot \Delta B^y \cdot \left(ct - ct_1 \cdot T + ct_2 \cdot T^2\right) \tag{2}$$

where ct, ct_1, ct_2 are the ferrite material's coefficients; T is the operating temperature of the core material

The parameters in Eq. 2 are defined for a selected magnetic material and valid only within a specific frequency range. The temperature dependant coefficients ct, ct_1 and ct_2 are selected so that the term in brackets yields 1 at $T = 100\,°\text{C}$.

As the plots are acquired for sinusoidal excitation rather than the triangular-shaped currents frequently present in power electronics, one must employ analytical tools and methods to make Eq. 2 applicable to a non-sinusoidal or arbitrary shape of the magnetizing current [7].

2. Temperature distribution in windings of gapped and ungapped magnetic components

It can be demonstrated that the extra power loss due to the fringing effect in the vicinity of the air gap is responsible for a distinctive pattern in temperature distribution in the winding if measured along the gapped column of the magnetic core. By mounting the same winding on an ungapped core formed out of a distributed-gap-type material one can show that this pattern is largely absent due to the fact that the fringing-effect power-loss mechanism is not present. The ungapped core should be of the same size and have an effective inductance matching the one displayed by the original core with a discrete air gap. Having satisfied the above requirements, one can be assured that the operating conditions of the component as a whole will not be affected, with the exception of a somewhat increased core loss that should be of negligible consequence to the temperature distribution in the winding.

Initially a 24-turn coil was mounted on an E42/21/15 core of 3F3 ferrite material [5] centre-gapped to 2.1 mm (Fig. 4). This configuration resulted in an inductance of about 95 µH. The constructed inductor was incorporated into a forward converter to take the role of an output inductor. The converter itself was run until the steady-state temperatures in the setup were reached. The thermogram registered at the thermal steady state of the magnetic component is presented in Fig. 2. Subsequently, the same coil was fitted on an ungapped EMS-0432115-060 core formed out of Sendust magnetic metal powder (Fig. 4). The component had an inductance corresponding to the one measured for the gapped inductor. Again, the converter with the modified inductor was run at exactly the same conditions

as previously until the thermal steady state of the component was attained (Fig. 5).

One can notice that the ends of the coil mounted on the gapped core show the lowest temperature, while the maximum temperature is registered in the area directly above the air gap (Fig. 6). In the case of the ungapped inductor power loss is distributed nearly uniformly, with no fringing-effect component (Fig. 7). As the operating conditions for both inductors were identical, the pattern observed in the coil mounted on the ferrite core can be attributed to the air gap in the magnetic path of the component and the fringing-flux power loss associated with it.

It can be assumed that the temperature distribution in the coil of the magnetic-powder core, if the convection cooling is

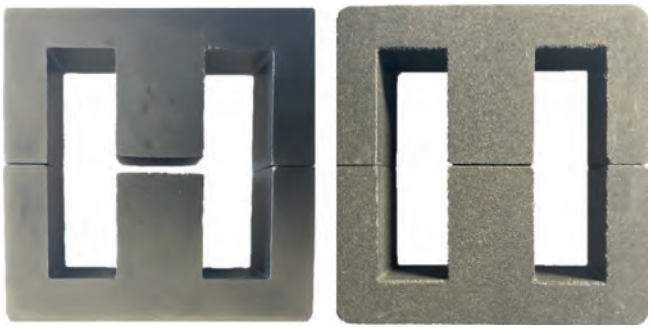

Fig. 4. Gapped ferrite core (left) and ungapped Sendust core (right)
Rys. 4. Rdzeń ferrytowy ze szczeliną powietrzną (po lewej) i rdzeń bez szczeliny wykonany z materiału Sendust (po prawej)

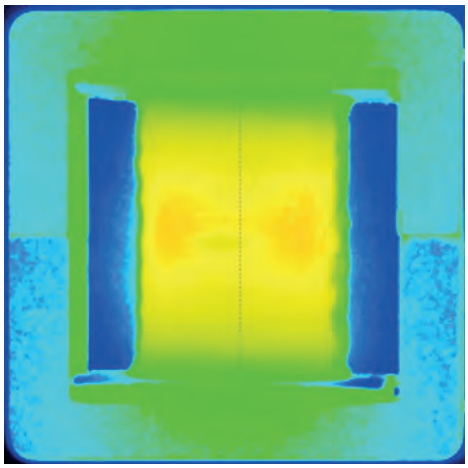

Fig. 5. Thermal image of ungapped inductor
Rys. 5. Obraz termowizyjny elementu indukcyjnego bez szczeliny

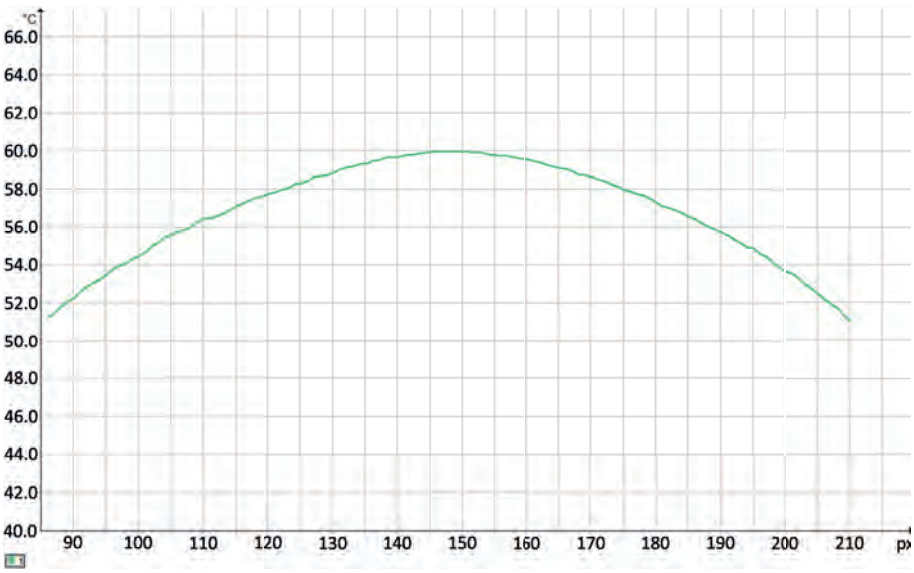

Fig. 6. Temperature distribution measured along middle column in gapped ferrite inductor of Fig. 2
Rys. 6. Rozkład temperatury wzdłuż środkowej kolumny w elemencie indukcyjnym ze szczeliną z Rys. 2

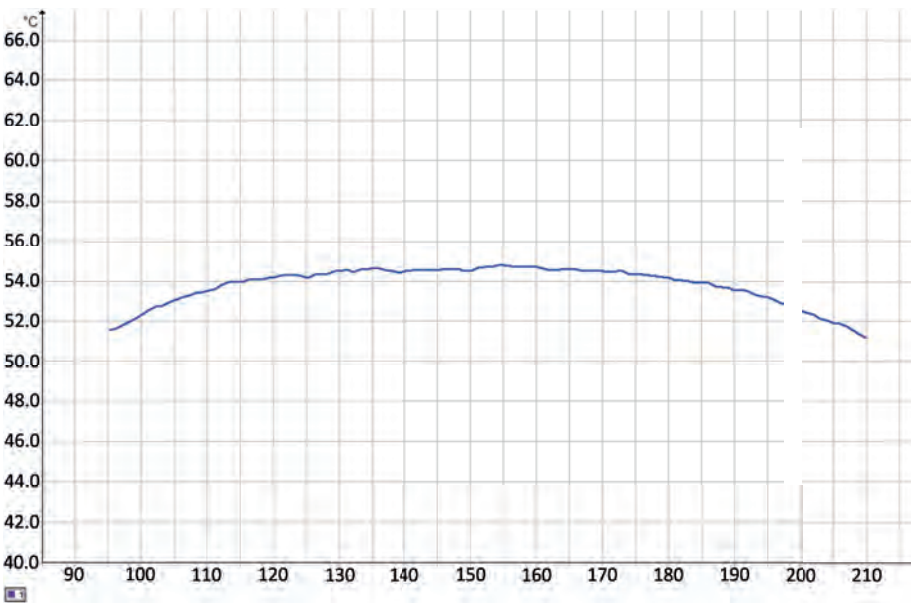

Fig. 7. Temperature distribution measured along middle column in ungapped magnetic-powder inductor of Fig. 5
Rys. 7. Rozkład temperatury wzdłuż środkowej kolumny w elemencie indukcyjnym bez szczeliny z Rys. 5

consistent along the winding, is solely governed by heat dissipation due to the current flow. This current, and its distribution within the wire, is a result of the input and output parameters of the converter, as well as the skin and proximity effects. As the fringing effect is not present, the power loss and temperature distribution in the winding are not determined by this factor. This observation can be utilized to ascertain the fringing-effect power loss in gapped magnetic components.

3. Extraction of fringing-effect power loss

Since ungapped magnetic components display a nearly homogenous power-loss density with no contribution from the fringing effect to the power loss, relating the total power dissipated in the examined ungapped inductor to the total power loss in the corresponding gapped component can facilitate the extraction of power dissipated exclusively due to the fringing--flux phenomenon.

Overall dissipation in the components can be ascertained by any suitable method. The approach employed herein is fairly straightforward and is based on calorimetric measurements. The investigated inductors were, one by one, suitably connected to the forward converter and positioned inside a sealed box (calorimeter). Subsequently, the converter was switched on and an increase in ambient temperature inside the box due to power dissipation in the components was monitored. The entire procedure starts with recording an initial internal ambient at the switch on of the converter and lasts until the thermal steady state inside the container is reached. At this point the internal steady state ambient is registered. In the next step, the component is substituted with a suitably selected resistor connected to a power source to reach the same increase in the internal ambient temperature, and hence the same power dissipated. It is crucial that throughout the experiment the external ambient remains unchanged. The power loss measurement setup is visualised in Fig. 8. The estimate of the total power dissipation might, to a certain and rather limited extent, differ from the factual power loss in the inductor as core loss and copper loss in coils is not temperature independent. The steady-state temperature inside the calorimeter is higher than the ambient in which the component typically operates. For that reason, it is of key importance to the accuracy of the measurements to select a suitable sealed container so that it provides a substantial reduction in convection cooling for apt changes in the internal ambient, and also offers a fitting trade-off between a sufficiently wide range of internal temperature variations and the impact it might have on power dissipation.

The total power loss evaluation process for the gapped inductor was initiated at an external, and also an internal, ambient of 27.0 °C. The whole procedure lasted the time needed to reach the thermal steady state for the inductor, at which point the ambient inside the container was registered as 32.5 °C. The subsequent measurement of power dissipation with a 100 Ω resistor showed that in order to arrive at exactly the same increase in the internal ambient approximately 1.646 W was required to be delivered from the power source.

The same setup was employed to get the estimate of the power loss in the ungapped inductor. In this case, at the moment of reaching the steady state, an internal ambient of 32.0 °C was registered, whereas the external ambient was the same as in the former case. This temperature rise translated into about 1.56 W dissipated in the 100 Ω resistor.

Power is being dispersed in both the magnetic core and the copper windings. Therefore, the total power loss obtained in the course of measurements can be separated into the corresponding categories. Power dissipated in ferromagnetic cores can frequently be ascertained with satisfactory accuracy using the data provided by manufacturers and a modified version of the Steinmetz equation, Eq. 2, so that it is applicable to the magnetic components with magnetizing currents of arbitrary shapes. The current and voltage waveforms for the examined inductors operating as the output choke in the forward converter are illustrated in Fig. 9. As the components had matching inductances their operating conditions were essentially identical, and hence had virtually the same current and voltage waveforms.

The values of the voltage across the inductor and the current flowing through the component at individual points in time throughout the switching period can be read from Fig. 9. As can be observed, channel 1 shows the voltage waveform and channel 3 denotes the current where 100 mV per division corresponds to 1 A. It has to be noted that for higher values of DC currents flowing through the inductors, and therefore higher magnetizing forces, the value of magnetic permeability and, by extension, inductance might be impacted differently in each of the components. This will cause certain discrepancies between individual current waveforms in the inductors.

Due to the fact that the current waveform is non-sinusoidal, it has to be replaced with an equivalent sinewave frequency by means of Eq. 3 [7] for a piecewise linear character of magnetic flux density B, where B_k and t_k denote values and time where a reversal in the magnetic flux density takes place.

$$f_{\sin_{eq}} = \frac{2}{\pi^2} \sum_{k\ 2}^{K} \left(\frac{B_k - B_{k\ 1}}{B_{\max} - B_{\min}} \right)^2 \cdot \frac{1}{t_k - t_{k\ 1}} \tag{3}$$

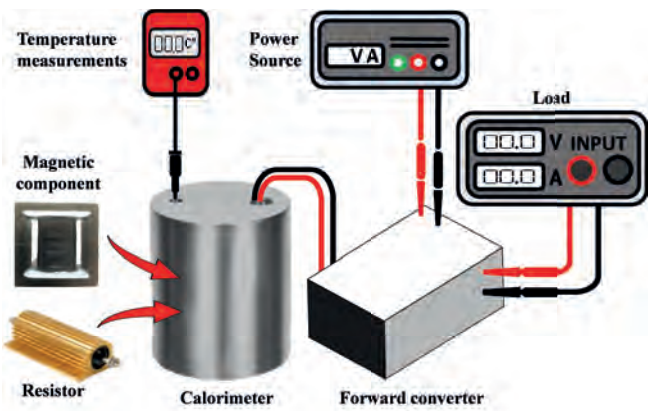

Fig. 8. Power loss measurement setup
Rys. 8. Układ do pomiaru strat mocy

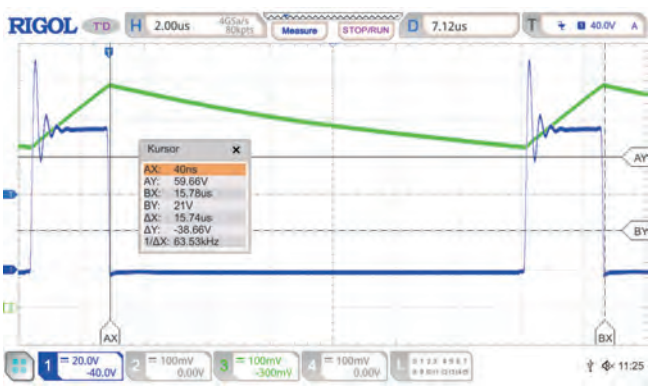

Fig. 9. Voltage (blue) and current (green) waveforms in examined inductors
Rys. 9. Przebiegi napięcia (niebieski) i prądu (zielony) dla badanych elementów indukcyjnych

For the waveforms of the switching period T_0 of 15.74 µs and the duty cycle D_0 of 16.5 %, (see Fig. 9) Eq. 3 returns Eq. 4:

$$f_{\sin_{eq}} = \frac{2}{\pi^2 \cdot T_0} \cdot \frac{1}{D_0 \cdot \left(1 - D_0\right)} = 95\ 500\ \text{Hz} \tag{4}$$

The equivalent sinewave frequency implemented into Eq. 2 as an operating frequency together with the peak AC flux density ΔB will yield the total core loss per unit volume for the inductors. The maximum AC value of ΔB can be derived from the waveforms of Fig. 9 and the construction parameters of the investigated magnetic components, Eq. 5.

$$\Delta B_{(peak-peak)} = \frac{V_{OUT} \cdot \Delta t}{N \cdot A_e} = \frac{11\,\text{V} \cdot 13.14\,\mu\text{s}}{24 \cdot 175 \cdot 10^{-6}\,\text{m}^3} = 0.035\ \text{T} \tag{5}$$

where Δt is the part of the switching period T_0 when the primary power switch of the forward converter is switched off; V_{OUT} is the converter's output voltage; N is the number of turns; A_e is the cross sectional area of the core used.

The peak AC flux density, Eq. 6:

$$\Delta B = \frac{\Delta B_{(peak-peak)}}{2} = 0.0175\ \text{T} \tag{6}$$

The 3F3 ferrite material coefficients, as read from the manufacturer's datasheets for a frequency range of 20–100 kHz [8], are: $k_f = 0.020005432$, $x = 2.009999955$, $y = 3.004999933$, $ct = 2.041666667$, $ct_1 = 0.020833333$, $ct_2 = 0.000104167$, and the mean operating temperature of the ferrite core was measured to be about 39.0 °C.

$$P_{V(3F3)} \cong 1.491\ \frac{\text{kW}}{\text{m}^3}$$

In order to obtain the actual core loss, the above power loss per unit volume has to be multiplied by the core effective volume V_e of the E42/21/15 core used in the construction of the inductor.

$$P_{(3F3)} = P_{V(3F3)} \cdot V_e = 1.491\ \frac{\text{kW}}{\text{m}^3} \cdot 17\ 300 \cdot 10^{-9}\text{m}^3 \cong 0.026\,\text{W}$$

One can infer that the vast majority of power dissipation occurs in the copper winding of the gapped-core inductor.

$$P_{Cu(3F3)} = P_{total(3F3)} - P_{(3F3)} = 1.646\ \text{W} - 0.026\ \text{W} = 1.62\,\text{W}$$

In the case of the ungapped EMS-0432115-060 core, total core loss per unit volume can be read from the graphs provided by the manufacturer [9] or obtained by the following curve fit formula [10], Eq. 7:

$$P_{V(EMS)} = \frac{f}{\frac{a}{\Delta B^3} + \frac{b}{\Delta B^{2.3}} + \frac{c}{\Delta B^{1.65}}} + d \cdot \Delta B^2 \cdot f^2 \tag{7}$$

where *a, b, c, d* are the Sendust material's coefficients [10].

The above equation requires peak AC flux density ΔB to be given in Gauss units and frequency f to be expressed in Hz. Therefore the peak AC flux density in Eq. 6 has to be multiplied by 10 000.

As previously, to arrive at the total power loss in EMS-0432115-060 core, the result yielded by Eq. 7 has to be multiplied by the core effective volume V_e.

$$P_{(EMS)} = P_{V(EMS)} \cdot V_e = 14.754\ \frac{\text{kW}}{\text{m}^3} \cdot 17\ 300 \cdot 10^{-9}\text{m}^3 \cong 0.255\,\text{W}$$

The manufacturer of the core formed out of Sendust magnetic metal powder does not disclose the data concerning the dependence of power loss in the material on temperature, and hence the actual power dissipation may somewhat deviate from the obtained figure.

The computed power loss in the core of the ungapped inductor was about tenfold the power dissipation in its gapped counterpart. Straightforward subtraction of the calculated core loss from the total power loss in the metal-powder magnetic component will yield the copper loss in the component.

$$P_{Cu(EMS)} = P_{total(EMS)} - P_{(EMS)} = 1.56\ \text{W} - 0.255\ \text{W} = 1.3\,\text{W}$$

The winding of the ungapped inductor does not experience the impact of the fringing field, so that the assumption that total power loss for the component has no fringing-effect element should be considered valid. Relating the total power losses measured in the windings of both examined magnetic components, one can obtain the estimate of the fringing-effect power loss in the gapped ferrite-core inductor. The entire difference in power dissipation between the two inductors can be attributed to the fringing-effect power loss:

$$P_{fring} = P_{Cu(3F3)} - P_{Cu(EMS)} = 1.62\ \text{W} - 1.3\ \text{W} = 0.32\,\text{W}$$

As one can infer, the total fringing-effect loss constitutes about 20 % of the total power loss in the winding of the inductor.

4. Conclusion

As demonstrated herein, power loss in a coil of a gapped magnetic component brought about only by the fringing effect can be ascertained by evaluating total power dissipated in the component and weighing it against total dissipation in its ungapped counterpart. Magnetic components mounted on distributed-gap-type core materials, due to the lack of physical discontinuity in their magnetic path, are not affected by eddy currents generated by the fringing flux, and hence no extra power loss is caused by the phenomenon. Substituting the discrete-gap core with the fully-distributed-type core of the same size may, ultimately, facilitate the extraction of the fringing-effect power loss.

Certain pragmatic precautions should be taken into account while applying the presented method to determine total power loss in the components. The thermal measurement ought to be carried out in invariable conditions and the results should be ensured to be as reliable as possible. Materials used in the construction of the magnetic components are not free of certain nonlinearities that may, to some degree, affect power dissipation and cause it to change over time. One of the sources of such uncertainty is the dependency of core loss and copper loss on temperature. This may somewhat impact the calorimetric measurements.

Acknowledgments

This research was funded by Narodowe Centrum Nauki as part of the MINIATURA 6 project, grant number – 562623, under registration number – 2022/06/X/ST7/01370.

References

1. Tian Y., Li Y., Liu J., *Fringing Field Analytical Calculation of High Frequency Planar Magnetic Components,* "CPSS Transactions on Power Electronics and Applications", Vol. 7, No. 3, 2022, 251–258, DOI: 10.24295/CPSSTPEA.2022.00023.

2. Kasikowski R., Więcek B., *Fringing-Effect Losses in Inductors by Thermal Modelling and Thermographic Measurements*, "IEEE Transactions on Power Electronics", Vol. 36, No. 9, 2021, 9772–9786, DOI: 10.1109/TPEL.2021.3058961.
3. Zaikin I.D., *Round and Tubular Wire Skin Effect Modeling and Usage SPICE as Maxwell's Equations Solver*. [In:] 23rd Telecommunications Forum Telfor (TELFOR), Belgrade, Serbia, 2015, DOI: 10.1109/TELFOR.2015.7377551.
4. Ngo K.D.T., Lu M., *Analytical Calculation of Proximity-Effect Resistance for Planar Coil With Litz Wire and Ferrite Plate in Inductive Power Transfer*, "IEEE Transactions on Industry Applications", Vol. 55, No. 3, 2019, 2984–2991, DOI: 10.1109/TIA.2018.2890366.
5. Ferroxcube Data Handbook, *Soft Ferrites and Accessories*, Ferroxcube, 2013, 120–121.
6. Steinmetz C.P., *On the Law of Hysteresis*, "Transactions of the American Institute of Electrical Engineers", Vol. 4, No. 1, 1892, 1–64, DOI: 10.1109/T-AIEE. 1892.5570437.
7. Albach M., Durbaum T., BrockmeyerT., *Calculating Core Losses in Transformers for Arbitrary Magnetizing Currents, A Comparison of Different Approaches*. [In:] 27th Annual IEEE Power Electron. Specialists Conf., Baveno, Italy, 1996, DOI: 10.1109/PESC.1996.548774.

Other sources

8. *Ferroxcube* [www.ferroxcube.com/upload/media/design/FXCStainmetzCoefficients.xls].
9. *Micrometals* [https://s3.amazonaws.com/micrometals-production/filer_public/2f/ed/2fedd6eb-44d0-4834-a442-8222486f0b77/micrometals_alloy-en-2021.pdf].
10. *Micrometals* [https://s3.amazonaws.com/micrometals-production/filer_public/62/c0/62c0d9d3-96f3-41c6-830e-35d5a8aab07e/mmcurvefitcoefficientsall-sept21.xlsx].

Wyodrębnienie strat mocy spowodowanych strumieniem rozproszenia z całkowitych strat mocy w elemencie indukcyjnym

Streszczenie: Elementy indukcyjne konwertujące i magazynujące moc elektryczną nie są w stanie przetworzyć znacznej ilości mocy bez wprowadzenia fizycznej nieciągłości w przestrzeń ich obwodów magnetycznych. Przerwa ta często przybiera formę dyskretnej szczeliny powietrznej, co pociąga za sobą pewne następstwa głównie w postaci dodatkowych start mocy w uzwojeniach tak skonstruowanych elementów indukcyjnych. Oszacowanie wpływu rozproszonego pola magnetycznego przy szczelinie powietrznej na sprawność przetwarzania energii jest bardzo problematyczne przede wszystkim ze względu na złożony charakter zjawiska. Ta dodatkowa strata mocy występuje zwykle wspólnie i łączy się z pozostałymi mechanizmami rozpraszania mocy, co znacznie komplikuje ekstrakcję strat spowodowanych wyłącznie przez strumień rozproszonego pola magnetycznego przy szczelinie powietrznej z całkowitej mocy rozproszonej w danym elemencie indukcyjnym. Rdzenie magnetyczne z materiałów kompozytowych nie wymagają dyskretnej szczeliny powietrznej, gdyż szczelina powietrzna jest w nich rozłożona w objętości całego materiału, a tym samym brakuje fizycznego mechanizmu powodującego powstawanie strumienia rozproszenia. Rozwiązanie to ma jednak wadę w postaci zwiększonych strat w materiale rdzenia. Jak zademonstrowano, rdzenie o szczelinie rozproszonej nie wykazują strat mocy spowodowanych strumieniem rozproszenia, a tym samym mogą stanowić podstawę do wyodrębnienia strat mocy wyłącznie z powodu tego zjawiska w elementach indukcyjnych z dyskretną szczeliną powietrzną.

Słowa kluczowe: cewki, dławiki, transformatory, termografia, straty mocy

Rafał Kasikowski, PhD Eng.
rafal.kasikowski@p.lodz.pl
ORCID: 0000-0002-2815-1746

He received the MSc degree in electrical engineering in 2002 from the Technical University of Czestochowa, Poland, and he has also earned the MSc degree in energy engineering in 2013 from the University of East Anglia, Norwich, United Kingdom. In 2021 he received the PhD degree in electronics from Lodz University of Technology, Poland, where he is currently working as a postdoctoral researcher. His research interests include modelling and optimization of magnetic components in Switch Mode Power Supplies.